Structural Changes in Cytochrome P-450$_{cam}$ Effected by the Binding of the Enantiomers (1*R*)-Camphor and (1*S*)-Camphor[†]

Heike Schulze,[‡] Gaston Hui Bon Hoa,[§] Volkhard Helms,[∥] Rebecca C. Wade,[∥] and Christiane Jung*,[‡]

MDC, Max-Delbrück-Centrum für Molekulare Medizin Berlin-Buch, Robert-Rössle-Strasse 10, 13122 Berlin, Germany, INSERM-U310, Institut de Biologie Physico-Chimique, 13 rue P. et M. Curie, 75005 Paris, France, and European Molecular Biology Laboratory Heidelberg, Meyerhofstrasse 1, 69012 Heidelberg, Germany

Received November 16, 1995; Revised Manuscript Received July 8, 1996[⊗]

ABSTRACT: A comparative study of the enantiomeric substrate [(1*R*)-camphor- and (1*S*)-camphor)-bound cytochrome P-450$_{cam}$ concerns the spin-state equilibrium, substrate dissociation, the thermal unfolding of the protein structure, and the subconformer equilibria observed in the infrared spectra of the carbon monoxide (CO) complex of cytochrome P-450$_{cam}$. The behavior of the different conformational equilibria in dependence on temperature, pressure, pH-value, cosolvent, and cation binding led us to suggest that (1*S*)-camphor is more loosely and less optimally bound in the heme pocket, which facilitates the access of solvent molecules into the heme-iron environment. The spin reaction volume difference measured using the high pressure technique is smaller by 16 ± 9 cm^3/mol for (1*S*)-camphor-bound P-450$_{cam}$ compared to the (1*R*)-camphor-bound P-450$_{cam}$, which might indicate a higher water content in the protein and in the heme environment in the (1*S*)-camphor complex. The half-transition temperature of the thermal unfolding of 53.8 °C for the (1*S*)-camphor-bound oxidized cytochrome P-450$_{cam}$ is one degree lower than the value for the (1*R*)-camphor-bound protein (54.8 °C). In the reduced, CO-bound form of cytochrome P-450$_{cam}$ at 290 K the (1*S*)-camphor complex reveals another CO stretch vibration population distribution with slightly higher frequencies [1940.2 cm^{-1} (major band) and 1946.3 cm^{-1} (minor band)] compared to the (1*R*)-camphor complex [1939.7 cm^{-1} (major band) and 1930 cm^{-1} (minor band)]. A loosening of the contact between the iron-bound CO ligand and amino acids of the I-helix, probably induced by compensating effects of the increased water content, is suggested. Assuming the carbon monoxide complex as a model for the dioxygen complex, the more loosened binding of (1*S*)-camphor, therefore the increased water accessibility, and the weaker contact of the iron ligand to the I-helix might explain the higher amount of uncoupling of the cytochrome P-450 reaction cycle compared to that when (1*R*)-camphor is used as substrate.

Cytochrome P-450 comprises a superfamily of heme-thiolate proteins, which catalyze hydroxylations of organic compounds of different nature. The genes of more than 200 members of this superfamily have been characterized (Nelson et al., 1993), and the crystal structure of four bacterial cytochrome P-450 proteins have been solved recently (Hasemann et al., 1995; Cupp-Vickery et al., 1994). Among the various members of the superfamily the (1*R*)-camphor-hydroxylating P-450$_{cam}$[1] is the best-studied P-450 protein from the biochemical, molecular biological, and biophysical points of view. Most of the basic ideas about the reaction mechanism are derived from studies on this P-450 protein (Raag & Poulos, 1992). Regarded earlier as a P-450 enzyme with strict substrate specificity compared to microsomal P-450, this picture has been changed in the last few years when hydroxylations of diverse substrates other than (1*R*)-camphor have been found (Kadkhodayan et al., 1995; De Voss & Ortiz de Montellano, 1995; Fruetel et al., 1994; Maryniak et al., 1993; Atkins & Sligar, 1988, 1989). This observation makes P-450 interesting for biotechnological applications when gene engineering tools are used to redesign the protein for modulated substrate specificity or increased hydroxylation efficiency (Fowler et al., 1994; Loida & Sligar, 1993a,b; Paulsen et al., 1993; Tuck et al., 1993; Atkins & Sligar, 1989). Inspite of the large amount of physico-chemical data collected over the years about structure−function relationships in P-450, a physically based strategy for redesigning a P-450 protein for the conversion of a specific substrate is still far from being clear. Detailed understanding of the effect of substrate binding on the changes of the protein structure, particularly near the

[†] This study was supported in part by the Deutsche Forschungsgemeinschaft (Ju229/3-1), the Deutscher Akademischer Austauschdienst in the frame of a PROCOPE project (312/pro-bmft-gg), the Agence pour l'organisation de l'accueil des personnalités étrangères (A.P.A.P.E.) in the frame of a PROCOPE project (94116), and by the European Community (BIO2-CT94-2060).

* Author to whom correspondence should be addressed. Tel: +49 30 9406 3370. Fax: +49 30 9406 3329. E-mail: cjung@orion.rz.mdc-berlin.de.

[‡] MDC.

[§] INSERM-U310.

[∥] European Molecular Biology Laboratory Heidelberg.

[⊗] Abstract published in *Advance ACS Abstracts,* August 15, 1996.

[1] Abbreviations: P-450$_{cam}$ cytochrome P-450$_{cam}$, soluble heme protein from *Pseudomonas putida* that catalyzes the hydroxylation of (1*R*)-camphor when utilized as the sole carbon source (EC 1.14.15.1; CYP 101; Nelson et al., 1993); (1*R*)-camphor, (1*R*)-(+)-camphor, D-camphor; (1*S*)-camphor, (1*S*)-(−)-camphor, L-camphor; ν(CO), frequency of the carbonmonoxy stretch vibration; $\Delta\nu_{1/2}$, bandwidth of the carbon monoxide stretch vibration absorption band; EPR, electron paramagnetic resonance; rms, root mean square.

S0006-2960(95)02730-9 CCC: $12.00

dioxygen binding site at the heme iron and in the I-helix groove, which has been suggested to be important for oxygen activation (Kimata et al., 1995; Harris & Loew, 1994; Poulos et al., 1987), are required.

Recently we have shown that deeper insight into the substrate-induced structural changes near the dioxygen binding site is obtained from Fourier transform infrared measurements of the stretch vibration mode of the carbon monoxide ligand in P-450$_{cam}$−CO (Jung et al., 1996; Schulze et al., 1994b; Jung et al., 1992; Jung & Marlow, 1987). A strong influence of the binding of various camphor analogues on the CO stretch vibration was observed (Legrand et al., 1995; Jung et al., 1992) and has been related to the mobility of the substrate in the heme pocket. Although this relation can be regarded as straightforward, unspecific and indirect effects of the different chemical properties of the substrate analogues (solubility, nature, and steric influence of functional groups) on the P-450 structure are hard to estimate.

For deeper understanding of the physico-chemical parameters studied, we were, therefore, looking for a substrate analogue which would bind in the heme pocket in a different geometry from (1*R*)-camphor but which would have the same chemical and physical properties as (1*R*)-camphor. The only substrate that fulfills this requirement is the optical antipode (1*S*)-camphor. Optical antipodes, in general, show the same physico-chemical properties like mass, size, dipole moments, polarizability, and solubility in nonchiral solvents. Their different behavior in chemical reactions results only from their different structural recognition by other molecules due to the mirror-symmetry of the enantiomer structure. We use, therefore, (1*S*)- and (1*R*)-camphor as three-dimensional probes of the active site of P-450$_{cam}$ to understand more clearly what information about the heme pocket we get from the physico-chemical parameters measured with different methods, in particular with infrared spectroscopy of the CO stretch mode.

In the present paper, we compare both (1*R*)- and (1*S*)-camphor complexes of P-450$_{cam}$ with regard to temperature, pressure and pH dependence of the heme iron high-spin/low-spin equilibrium, substrate dissociation constants, specificity of cation binding, thermal unfolding of the protein structure, and dependence of the CO stretch mode of the carbon monoxide ligand on the pH value, cation binding, cosolvent and temperature. From these studies, we conclude that (1*S*)-camphor is more loosely bound in the heme pocket than (1*R*)-camphor, which may facilitate water exchange between the solvent and the heme pocket. The slightly but distinctly higher frequencies of the CO stretch modes in the (1*S*)-camphor P-450$_{cam}$ complex are explained by a slightly weaker contact of the CO ligand to the I-helix (Jung et al., 1996), which might also be the case in the dioxygen complex. Both effects together may explain the observed 11% uncoupling of the P-450 reaction cycle from insertion of the oxygen atom into (1*S*)-camphor (Kadkhodayan et al., 1995; Maryniak et al., 1993) compared to only 3% when (1*R*)-camphor is used as substrate.

MATERIALS AND METHODS

Materials. Cytochrome P-450$_{cam}$ from *Pseudomonas putida* expressed in *Escherichia coli* TB1 was isolated and purified according to Jung et al. (1992). Camphor was removed by dialysis and column chromatography according to Jung et al. (1992) to obtain the substrate-free protein. Aqueous and ethanolic solutions of (1*R*)-camphor and (1*S*)-camphor, which were purchased from Sigma and Merck, respectively, and used without further purification, were added to the substrate-free protein. Glycerol was from Riedel-de-Haen.

Methods and Instrumentation. The residual water content as well as the water content in the dialysis solutions were determined by refractometry. The pH value of the buffer used for the dialysis solution was measured at 23 °C with a pH meter (Knick 761 Calimatic) or otherwise noted. The pH values of the dialysis solutions have to be corrected for the glycerol contribution. For 20% (by mass) glycerol solution, the real pH value shifts by 0.05 units to higher values and for 60% (by mass) glycerol by about 0.15 units (Douzou, 1977).

Analysis of the High-Spin/Low-Spin Equilibrium. The high-spin/low-spin equilibrium of the heme iron in oxidized P-450$_{cam}$ was monitored on the heme electronic absorption spectrum in the Soret band region. The high- and low-spin states show Soret band absorption maxima at 392 and 417 nm, respectively. The determination of the population of the high-spin state of the P-450$_{cam}$ samples is based on curve fitting the high-spin/low-spin mixed electronic absorption spectrum with the pure high-spin and pure low-spin states. Analytical functions for the pure high-spin and pure low-spin states (linear combinations of Gaussian bands) were constructed by Jung et al. (1991). A typical decomposed spectrum is presented in the insert of Figure 2. The concentration of P-450$_{cam}$ was 3−5 μM in 0.1 M potassium phosphate buffer, pH 7.0, and 400 μM of (1*R*)- or (1*S*)-camphor or as otherwise noted.

Temperature Dependence. The high-spin/low-spin equilibrium was studied at atmospheric pressure using Peltier-thermostated sample cells regulated with a TSK 200 temperature controller (Wissenschaftlicher Gerätebau Berlin) with a temperature stability of 0.1 K. Low-temperature studies were carried out using the cryostat DN 704 (Oxford), adapted to the spectrophotometer UV 2101PC (Shimadzu), regulated by the temperature controller DTC-2 (Oxford) with a temperature stability of 0.2 K. To obtain a glassy sample at low temperatures these studies were performed with a buffer−glycerol (60% by mass) mixture. Thermodynamic parameters for the temperature dependence of the spin equilibrium constant $K_{spin} = [P\text{-}450^{os}_{HS}]/[P\text{-}450^{os}_{LS}]$ were obtained from fitting the logarithm of the K_{spin} values against the reciprocal temperature using a least-squares fit program. The abbreviations o, s, LS, and HS refer to the oxidized, substrate-bound, low-spin, and high-spin states, respectively.

Pressure Dependence. Studies of the dependence on hydrostatic pressure were done in potassium phosphate buffer, pH 7.7, having different glycerol contents (0%−60% by mass). The measurements were taken on the Cary-219 spectrophotometer interfaced to a high-pressure bomb (Hui Bon Hoa et al., 1982a). Spectra were recorded with the data acquisition and fitting software package SpectraLab (Davydov et al., 1995). Thermal regulation of the pressure bomb at 277 K was provided by a thermostated circulating bath (Huber HS 40) allowing a temperature control of 0.5 K. Samples were first compressed to 20 MPa for 3 min, and the pressure was released to 0.1 MPa before starting the pressure study. Pressure was applied up to 600 MPa by 20 MPa increments. Spectra were recorded after 3 min of

equilibration. All absorption spectra were corrected for compression.

The volume difference ΔV_{spin} is given by $\Delta V_{spin} = -RT(\mathrm{d}\ln(1/K_{spin})/\mathrm{d}P)$ with K_{spin} being the spin-state equilibrium constant $K_{spin} = [\text{P-450}^{os}{}_{HS}]/[\text{P-450}^{os}{}_{LS}]$. The high-spin content was evaluated by the fitting program described by Jung et al. (1991). The pressure at half-transition $P_{1/2}$ ($K_{spin} = 1$) and the volume difference ΔV_{spin} were obtained from fitting the logarithm of K_{spin} against P in the pressure range 30−135 MPa in solutions with 0% (by mass) glycerol using a least-squares fit program. At higher glycerol contents the pressure range was shifted to higher values [170−300 MPa for 60% (by mass) glycerol] for fitting the logarithm of K_{spin} against P. The free energy was calculated by $\Delta G^{V} = P_{1/2}\Delta V_{spin}$.

Glycerol Effect. The studies of the glycerol effect were done at 277 and 297 K in 0.1 M potassium phosphate buffer, pH 7.0, with different glycerol contents (0%−60% by mass).

pH Dependence. The pH dependence of the spin equilibrium was studied with the P-450_{cam} samples before the samples were reduced and before the CO complex was formed for the pH dependence measurements of the CO stretch vibration.

EPR Measurements. The high- and low-spin states were also characterized at atmospheric pressure using EPR measurements carried out using the E300 spectrometer (Bruker) with a modulation amplitude of 31.887 G, a microwave power of 50.2 mW and a modulation frequency of 100 kHz. EPR *g*-values were calculated for the field set (2500−4000 G). For slow-cooling experiments (0.3 K/min) the sample in the EPR tube was brought to the target temperature (78 K) using the Oxford cryostat before being transferred to the EPR spectrometer. For the fast-cooling experiments the sample was frozen in by the common method of immersion into liquid nitrogen, which corresponds to a cooling rate of approximately 1000 K/min. The protein and substrate concentrations were 1.1−1.7 and 4 mM, respectively.

Determination of Substrate Dissociation Constants. Substrate-free P-450_{cam} (with a 100% low-spin content) was titrated with (1*R*)- or (1*S*)-camphor by stepwise addition of the substrate solution to the protein solution using a microsyringe and monitoring the Soret band absorption spectrum change from the low-spin to the high-spin state. Measurements were performed on the UV 2101PC (Shimadzu) spectrophotometer at various set temperatures.

Using the Hill equation (eq 1) the apparent substrate dissociation constant K_d with $K_d = [\text{P-450}^{o}{}_{LS}][S]/([\text{P-450}^{os}{}_{HS}] + [\text{P-450}^{os}{}_{LS}])$ was determined considering the total substrate concentration [S(total)], the protein concentration [protein], the dilution factor, and the extinction differences between 392 and 417 nm in the substrate-induced absorption difference spectra (ΔE).

$$\Delta E = \frac{\Delta E_{max}[S]^{n}}{K_d + [S]^{n}} \quad (1)$$

[S] is described by $[S] = [S(total)] - [protein]\Delta E/\Delta E_{max}$. The Hill coefficient n is fitted and ranges between 0.9 and 1.1. The maximal extinction difference between 392 and 417 nm in the substrate-induced absorption difference spectra (ΔE_{max}) at substrate saturation is also fitted.

Thermodynamic parameters for substrate dissociation were obtained from fitting the K_d values at different temperatures using eq 2.

$$K_d = \exp[-\Delta H_d/RT + \Delta S_d/R - \Delta C_p(1 - T/T_0 - \ln(T/T_0))/R] \quad (2)$$

The enthalpy change for the substrate dissociation is described by ΔH_d, the entropy change by ΔS_d, the heat capacity by ΔC_p, and T and T_0 are the temperature and the standard temperature (291.52 K), respectively. ΔC_p can be set to zero in the small temperature range we used. Measurements were done in 0.1 M potassium phosphate buffer, pH 7.0, as well as in a buffered glycerol mixture [60% (by mass) glycerol].

Determination of Cation Binding Constants. Addition of cations increases the high-spin content. The apparent dissociation constant $K_{d,cat} = [\text{P-450}^{os}][cation]/[\text{P-450}^{os}\cdot cation]$ for the cation−protein interaction was estimated in the same way as described for the substrate dissociation studies. Measurements were done according to Deprez et al. (1994b) at 293 K in 50 mM Tris-HCl buffer, pH 7.0 (293 K), containing 400 μM camphor.

Thermal Unfolding. The optical spectra for the thermal unfolding studies were taken on the Jasco V550 spectrophotometer in the temperature range from 297 to 366 K. The temperature was adjusted in the cell using a thermostat (Haake DC1). The thermodynamic parameters were calculated from the decrease of the Soret band at 392 nm [$\Delta E(T)$] using the integrated van't Hoff equation (eq 3).

$$\Delta E(T) = \frac{A + BT + (C + DT)\exp[-\Delta H_u(1/T - 1/T_{1/2})/R]}{1 + \exp[-\Delta H_u(1/T - 1/T_{1/2})/R]} \quad (3)$$

The fit parameters *A*, *B*, *C*, and *D* consider the slope of the linear shift, which might be superimposed on the S-shaped behavior. ΔH_u is the enthalpy change of the protein unfolding, and T and $T_{1/2}$ are the temperature and the half-transition temperature, respectively. ΔS_u is the entropy change of the protein folding and is calulated by $\Delta H_u/T_{1/2}$.

Measurements of the CO Stretch Vibration Using Infrared Absorption Spectroscopy. For the infrared absorption spectroscopic studies, the final concentration of the P-450_{cam}−CO complex was 0.8−1.4 mM, which was determined from the Soret band absorption measured directly in the infrared cell on the spectrophotometer UV 2101PC (Shimadzu) and using the absorption coefficient at 446 nm of 127 mM^{-1} cm^{-1} (Gunsalus & Sligar, 1978). For the preparation of the infrared samples the protein was concentrated to 1.3 mM and dialyzed against a solution of a definite pH value, monovalent cation concentration, or glycerol content. For all measurements, the carbon monoxide complex of P-450_{cam} was prepared as published elsewhere (Schulze et al., 1994b). The infrared cell consists of two calcium fluoride windows separated by a 0.1 mm thick Teflon spacer.

For the studies of the dependence of the CO stretch mode on the pH value, the composition of the aqueous dialysis solution was 20% (by mass) glycerol and 0.1 M potassium ions in 0.1 M phosphate or citrate phosphate buffer. For the measurements with different monovalent cation concentrations the mixture contained 20% (by mass) glycerol and 50 mM Tris-HCl buffer, pH 7.5. Temperature dependence

Table 1: Temperature Dependence of Spin-State Equilibrium in (1*R*)-Camphor- and (1*S*)-Camphor-Bound P-450$_{cam}$ and of Substrate Dissociation

	0% (by mass) glycerol		60% (by mass) glycerol	
	(1*R*)-camphor	(1*S*)-camphor	(1*R*)-camphor	(1*S*)-camphor
K_{spin} 277 K	31 ± 7	7.1 ± 0.3	74 ± 14	79 ± 19
K_{spin} 297 K	251 ± 52	87 ± 37	1267 ± 286	1033 ± 94
ΔH_{spin} (kJ/mol), 220−270 K	−	−	74 ± 2	65 ± 2
ΔS_{spin} (J/mol K), 220−270 K	−	−	310 ± 10	271 ± 10
ΔH_{spin} (kJ/mol), 277−303 K	71 ± 11	84 ± 16	97 ± 14	88 ± 5
ΔS_{spin} (J/mol K), 277−303 K	285 ± 38	320 ± 58	386 ± 49	354 ± 15
K_d (μM), 277 K	2.2 ± 0.3	2.8 ± 0.1	2.3 ± 0.2	7.4 ± 0.9
K_d (μM), 297 K	0.8 ± 0.3	1.2 ± 0.1	1.4 ± 0.1	4.7 ± 0.3
ΔH_d (kJ/mol), 277−284 K	−49 ± 4	−40 ± 3	−	−
ΔS_d (J/mol K), 277−284 K	−286 ± 17	−252 ± 9	−	−
ΔH_d (kJ/mol) 284−303 K	−24 ± 2	−12 ± 6	−	−
ΔS_d (J/mol K), 284−303 K	−196 ± 7	−155 ± 19	−	−

studies were done with samples in 20% and 60% (by mass) glycerol and 0.1 M potassium phosphate buffer, pH 7.0. The dialysis buffers contained at least 1 mM camphor.

Enthalpy and entropy values (298 K, 0.1 MPa) are obtained from global fit analysis of the relative band area (Jung & Marlow, 1987; Frauenfelder et al., 1990, Jung et al., 1996).

Infrared spectra were recorded on the Bruker IFS 66 Fourier transform infrared spectrometer with a liquid nitrogen cooled mid-band MCT detector in the double-sided/forward−backward acquisition mode at 2 cm^{-1} resolution. Fourier transformation of the interferogram was performed with a zero-filling factor of 2 and the Happ−Genzel apodization function. 200 interferograms were accumulated. For the pH and the cation effect studies the spectra were taken at a constant temperature of 28.5 °C.

Low-temperature measurements were performed with a closed-cycle helium refrigerator (Cryogenics model 22) and a Lake Shore Cryotronics DRC-91CA temperature controller. A silicon diode mounted on the sample cell monitored the temperature. All temperature-induced spectral changes were completely reversible in many cycles.

Infrared absorption spectra were obtained from the ratio of the intensity spectrum for the protein CO complex to the intensity spectrum of the dialysis buffer. In most cases a completely flat base line was not observed. Therefore, the infrared absorption spectra of the sample were further corrected by subtracting interactively the absorption spectrum of the dialysis buffer until an almost flat base line was obtained (Schulze et al. 1994b). Additionally, the base line correction was improved by fitting the right and left sides of the spectrum outside from the absorption band using a cubic polynomial. All base line-corrected absorption spectra were decomposed with a nonlinear least-squares curve fit procedure written in Turbo Pascal by O. Ristau using Gaussian line shapes (Schulze et al., 1994b).

RESULTS

A comparative analysis of the influence of enantiomeric substrates [(1*R*)- and (1*S*)-camphor] on the active site of cytochrome P-450$_{cam}$ is presented using spectroscopic markers. First, we used the Soret band of the ferric heme-iron of P-450$_{cam}$. We investigated the temperature and pressure dependence of the spin-state equilibrium of the oxidized form of cytochrome P-450$_{cam}$ and its behavior with changes of the pH value, the cation concentration and glycerol content. Substrate binding behavior is analyzed by determination of dissociation constants. Temperature jump kinetics of the high-spin to low-spin transition and thermal unfolding of the protein were performed. The second spectroscopic marker we used is the infrared band resulting from the CO stretch mode of the ferrous heme-iron CO complex. This marker is investigated concerning its change with temperature, glycerol content, pH, and cation concentration. The comparison of the results obtained for the ferric and ferrous P-450−CO should give deeper insights in the structural differences between (1*R*)- and (1*S*)-camphor-bound P-450$_{cam}$.

Thermodynamics of Spin-State Equilibrium: Temperature Dependence. Table 1 summarizes the equilibrium constants and thermodynamic parameters of the high-spin/low-spin equilibrium for the (1*R*)-camphor and the (1*S*)-camphor complexes of P-450$_{cam}$ under saturating substrate concentrations in aqueous and glycerol containing buffered solution.

In Aqueous Solution. In the absence of glycerol the high-spin state is significantly more favored in the (1*R*)-camphor complex than in the (1*S*)-camphor complex. The spin-state equilibrium constant K_{spin} is 3−4-fold larger for (1*R*)-camphor-bound P-450$_{cam}$ than for (1*S*)-camphor-bound P-450$_{cam}$. In other words, (1*R*)-camphor-bound P-450$_{cam}$ is 98% in the high-spin state at 277 K while (1*S*)-camphor-bound P-450$_{cam}$ shows a high-spin content of only 88%.

In the temperature range 277−303 K we found similar enthalpy and entropy values for both enantiomer complexes considering the experimental accuracy. The transition from the low-spin to the high-spin state is entropy-driven for both enantiomer complexes of P-450$_{cam}$ (Table 1). The thermodynamic parameters were calculated as mentioned in Materials and Methods. To compute K_{spin}, we determined the high-spin content from the curve fitting of the electronic absorbance spectrum (Jung et al., 1991) as well as measured the absorbance change with the optical difference spectroscopy according to Fisher and Sligar (1987). The reported experimental errors arise from the small change in the high-spin content for both enantiomer complexes [for (1*S*)-camphor from 88% to 99.4% and for (1*R*)-camphor from 98% to 99.8%] in the small temperature range (277−303 K).

Glycerol Effect. Studies at various glycerol contents in the buffered solution indicate that the high-spin state is favored by glycerol. K_{spin} and the thermodynamic parameters for both enantiomers increase on going to 60% (by mass) glycerol. However, the glycerol effect is more pronounced in the (1*S*)-camphor-bound P-450$_{cam}$. The addition of glycerol by up to 30% (by mass) to the (1*S*)-camphor-bound P-450$_{cam}$ leads to an increase of the high-spin content from

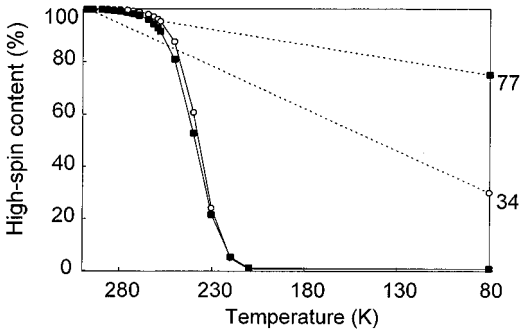

FIGURE 1: Percentage of high-spin as function of the temperature at (—) slow (0.3 K/min) and (- - -) fast (21 K/min) cooling rates. For slow cooling the sample is frozen step by step waiting for the equilibrium state. Fast cooling means the immersion of the sample into the precooled (78 K) chamber and waiting 12 min to freeze the sample from 298 to 78 K. (■) (1*R*)-Camphor- and (○) (1*S*)-camphor-bound P-450$_{cam}$, in 0.1 M potassium phosphate pH 7.0, 60% (by mass) glycerol, and saturating substrate concentration, 400 μM.

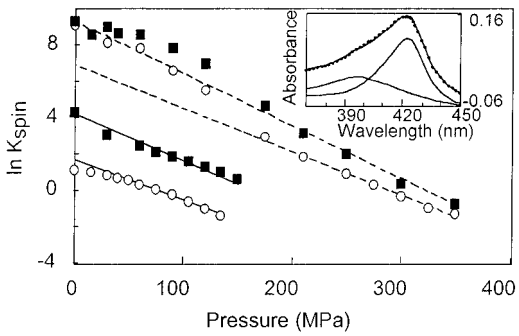

FIGURE 2: Plot of the logarithm of the spin equilibrium constant K_{spin} versus the hydrostatic pressure. (■) (1*R*)-Camphor- and (○) (1*S*)-camphor-bound P-450$_{cam}$, in 0.1 M potassium phosphate, pH 7.7, (—) 0% and (---) 60% (by mass) glycerol, saturating substrate concentration 400 μM. Values of ln K_{spin} higher than 5.5 are not considered for the evaluation of the thermodynamic parameters because of the uncertainty in evaluating the high-spin content in the range 99.6%−100%. Inset: The experimental (···) and fitted (—) electronic absorption spectrum of (1*R*)-camphor-bound P-450$_{cam}$ at 350 MPa in 60% (by mass) glycerol, 0.1 M potassium phosphate, decomposed into the contributing pure high-spin and pure low-spin bands.

93.8% to 98.8% at 277 K, while for the (1*R*)-camphor-bound P-450$_{cam}$ the high-spin content increases only from 97% to 98.7%.

We analyzed the spin-state transition in 60% (by mass) glycerol in the wider temperature range 220−270 K, because glycerol acts as a freeze-preventing solvent (Table 1). For both enantiomer complexes the high-spin content decreases from about 99.9% to 6%−9% high-spin content (Figure 1) on decreasing the temperature step by step from 295 to 180 K (0.3 and 3−5 K/min around the glass transition temperature). Comparing enthalpy and entropy values of the enantiomer complexes we found that (1*S*)-camphor-bound P-450$_{cam}$ reveals slightly lower thermodynamic values for the spin transition compared to (1*R*)-camphor-bound P-450$_{cam}$.

Kinetic Aspects of Spin Conversion Detected by Electronic Absorption Spectroscopy: Negative Temperature Jump Experiments. While the equilibrium parameters for the population of the high-spin and the low-spin states indicate only moderate differences between the enantiomer complexes, a remarkably different behavior is observed in the kinetics of the transition from the high-spin state to the low-spin state during cooling. When the sample is transferred from room temperature into the precooled thermostat at 78 K, a cooling rate of 21 K/min is applied. This fast cooling traps 77% of the high-spin state population in (1*R*)-camphor-bound P-450$_{cam}$; however, only 34% is trapped in (1*S*)-camphor-bound P-450$_{cam}$ (Figure 1). A measure for the kinetics can be defined by the slope (s) of the high-spin conversion from 295 to 78 K [s = ([P-450$^{os}{}_{HS(295K)}$] − [P-450$^{os}{}_{HS(78K)}$])/(295 K −78 K)]. The slope is tripled with (1*S*)-camphor [0.1 and 0.3 for (1*R*)- and (1*S*)-camphor, respectively], indicating a faster conversion to the low-spin state for the (1*S*)-camphor complex.

Kinetic Aspects of Spin Conversion Detected by EPR Spectroscopy: Negative Temperature Jump Experiments. To check whether both enantiomer complexes have the same nature of the high- and the low-spin states, the EPR spectrum was recorded. The slowly cooled samples (0.3 and 3−5 K/min around the glass transition temperature) have the same EPR spectrum for both enantiomers with *g*-values of 2.45/2.26/1.92 for the low-spin state (I) and *g*-values of 7.85/3.97/1.78 for the high-spin state, which is also detectable despite its small population. Very fast cooling by immersion of the EPR tube into liquid nitrogen (estimated cooling rate of approximately 1000 K/min) results in higher contributions of the high-spin state population in the EPR spectrum, which is more pronounced for the (1*R*)-camphor complex. The *g*-values are not changed. However, as already described by Schulze et al. (1994c) for (1*R*)-camphor-bound P-450$_{cam}$, an additional low-spin state (II) with *g*-values of 2.42/2.26/1.98 is also observed for the (1*S*)-camphor complex. While for (1*R*)-camphor-bound P-450$_{cam}$ this low-spin state (II) can also be detected by optical spectroscopy at 400 nm during fast cooling with a rate of 21 K/min (Schulze et al., 1994a), we failed to see this 400 nm absorbing species in the (1*S*)-camphor-bound P-450$_{cam}$. Obviously, this cooling rate is still too low to catch this nonequilbrium state.

Thermodynamics of Spin-State Equilibrium: Pressure Dependence. While the temperature effect on the equilibrium parameters of the spin states is not so strongly different in both enantiomer complexes, remarkable differences are observed in the behavior toward changes in the hydrostatic pressure. The increase of hydrostatic pressure up to a value where P-420 formation can still be neglected shifts the spin equilibrium toward the low-spin state. Figure 2 presents the decreasing values of ln K_{spin} with increasing hydrostatic pressure in 0% and 60% (by mass) glycerol. The insert shows the experimental and fitted spectrum of (1*R*)-camphor complex at 350 MPa with the pure high-spin and pure low-spin analytical functions. The frequency of the whole spectrum is shifted by 80−100 cm^{-1} to lower values with pressure (Jung et al., 1995). As demonstrated in Table 2 the pressure value at half-transition ($P_{1/2}$) is significantly lower for the (1*S*)-camphor complex compared to the (1*R*)-complex. Furthermore, the spin reaction volume difference between the high-spin state and the low-spin state is lower in the (1*S*)-camphor complex compared to (1*R*)-camphor complex at 0% glycerol. The spin reaction volume difference between the (1*S*)- and (1*R*)-camphor complex can be approximately estimated to 16 ± 9 cm^3/mol. The mean error of this difference arises from the mean error of ΔV_{spin} of the (1*S*)-camphor complex determined by separate calculation of ΔV_{spin} values for the pressure regions 15−90 and 30−135 MPa. The values of ln K_{spin} at low pressure were not

Table 2: Pressure Dependence of the Spin-State Equilibrium in (1*R*)- and (1*S*)-Camphor-Bound Oxidized P-450$_{cam}$

glycerol (%) by mass	$P_{1/2}$ (MPa)		ΔV_{spin} (cm^3/mol)		ΔG^V (kJ/mol)	
	(1*R*)- camphor	(1*S*)- camphor	(1*R*)- camphor	(1*S*)- camphor	(1*R*)- camphor	(1*S*)- camphor
0	175 ± 19	78 ± 6	−52 ± 3	−36 ± 6	−9.1	−2.8
20	231 ± 15	129 ± 7	−62 ± 2	−47 ± 2	−14.3	−6.0
40	267 ± 21	200 ± 8	−64 ± 3	−50 ± 1	−17.1	−10.0
60	305 ± 13	288 ± 18	−70 ± 2	−57 ± 2	−21.3	−16.4

included in the fit because we observed in several measurements that the first points often fall outside the line (Hui Bon Hoa and Jung, personal communication). In the case of higher glycerol content the uncertainty in evaluation the high-spin content in the range 99.6%−100% (ln K_{spin} is higher than 5.5) led to exclude the initial ln K_{spin} values from the correlation against pressure. Increasing glycerol concentration up to 60% increases $P_{1/2}$ and ΔV_{spin} but diminishes slightly differences in $P_{1/2}$ and ΔV_{spin} between the enantiomers.

The pH of phosphate buffer diminishes by about 0.4 units (Hui Bon Hoa & Marden, 1982b) on increasing the pressure, and one might expect an indirect pH effect on the spin transition of P-450$_{cam}$. However, under the set experimental conditions, the decrease of the pH from 7.7 to 7.3 is still in the pH range where a pH-induced high-spin to low-spin transition can be neglected (Schulze et al., 1994b). Therefore the pressure-induced pH change does not cause a significant shift of the spin equilibrium from the high-spin to the low-spin state, although it is in the same direction.

pH Dependence of Spin-State Equilibrium. Decreasing the pH value of the buffer from 7.8 to 4.8 induces the low-spin state in both enantiomer P-450$_{cam}$ complexes. This change follows an S-shaped behavior with a p*K* of 6.0 for (1*R*)-camphor (Schulze et al., 1994b) and a p*K* of 5.9 for (1*S*)-camphor.

Specificity of Cation Binding on Spin-State Equilibrium. Monovalent cations (lithium, sodium, potassium, rubidium, caesium) have a specific effect on the high-spin/low-spin equilibrium. Higher cation concentrations result in an increase of the high-spin content for both enantiomers but to different extents. In the Tris-HCl-buffered solution without monovalent cations the high-spin content in the (1*S*)-camphor-bound P-450$_{cam}$ is only 40%−45% (Figure 3), in contrast to 70% observed for (1*R*)-camphor-bound P-450$_{cam}$ (Deprez et al., 1994a). Preferential binding of potassium has been found in (1*R*)-camphor-bound P-450$_{cam}$ (Deprez et al., 1994a), resulting in 100% population of the high-spin-state. For (1*S*)-camphor, however, potassium and rubidium induce the spin-state equilibrium change to nearly complete high-spin state (99.9%).

As Deprez et al. (1994a) discussed for the (1*R*)-camphor complex, the rather large cations like rubidium and caesium are more effective at inducing the conformational change and increasing the high-spin content compared with lithium and sodium. Similar results were found for the (1*S*)-camphor complex (Table 3). However, Figure 3 clearly illustrates the difference in the cation binding behavior in the enantiomer complexes. The cation dissociation constants and the cation saturation concentrations are higher for (1*S*)-camphor compared to (1*R*)-camphor as shown in Table 3. Both enantiomer complexes show, however, the same qualitative dependence of these parameters on the cation radius. The amount of high-spin state population for saturating concentration of a given cation is almost the same for (1*R*)- and (1*S*)-camphor.

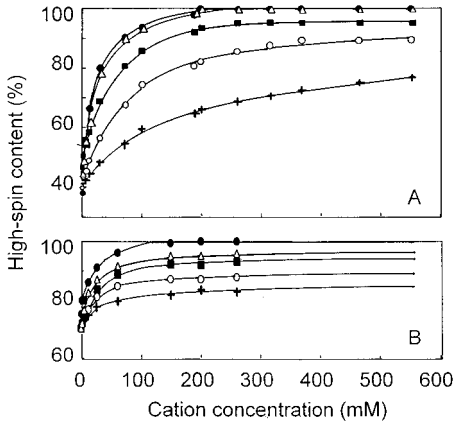

FIGURE 3: Percentage of high-spin as function of the cation concentration. (A) (1*S*)-Camphor-bound P-450$_{cam}$ in comparison to (B) (1*R*)-camphor-bound P-450$_{cam}$ refitted data from Deprez et al. (1994a). (●) K^+, (△) Rb^+, (■) Cs^+, (○) Na^+, (+) Li^+. Studies were done at 4 °C, in 50 mM Tris-HCl, pH 7.0, and 400 μM substrate.

Substrate Dissociation. The apparent substrate dissociation constants (K_d) for 277 and 297 K and the thermodynamic parameters (ΔH_d, ΔS_d) for the substrate dissociation are given in Table 1. The plot of the logarithm of the apparent dissociation constant K_d versus the reciprocal temperature reveals a different slope for (1*R*)-camphor as well as for (1*S*)-camphor in the temperature ranges of 277−287 and 287−303 K (Figure 4). This finding for (1*R*)-camphor agrees with data from Griffin and Peterson (1972) and Deprez et al. (1994b). In the presence of 60% (by mass) glycerol, the apparent dissociation constants in both enantiomer complexes are slightly increased (Table 1). Calculations of the free energy ΔG_d (from the enthalpy and entropy values given in Table 1 for the dissociation) reveal that the binding of both enantiomers is entropy-driven as already shown for (1*R*)-camphor by Deprez et al. (1994b).

Thermal Unfolding. As shown by Jung et al. (1985) and Nölting et al. (1991) substrate binding to substrate-free P-450$_{cam}$ stabilizes the protein structure against thermal unfolding. The half-transition temperature shifts from 40 °C for substrate-free P-450$_{cam}$ (Jung et al., 1985) to 54.8 ± 0.1 °C and 53.8 ± 0.1 °C after binding of (1*R*)- and (1*S*)-camphor, respectively. In both enantiomer complexes the unfolding is not reversible. Although equilibrium conditions are not given, we estimated the enthalpy and entropy values for the unfolding: (1*R*)-camphor, ΔH_u = 233.6 ± 12 kJ/mol, ΔS_u = 712.3 ± 0.3 J/K mol; (1*S*)-camphor, ΔH_u = 267.0 ± 15 kJ/mol, ΔS_u = 816.7 ± 0.3 J/K mol.

Ferrous Heme-Iron−CO Complex CO Stretch Vibration: Temperature Dependence. Figure 5 shows the infrared spectra for the CO stretch vibration. For both enantiomer P-450$_{cam}$−CO complexes the absorption bands are asym-

Table 3: Parameter of Cation Binding and Dissociation in (1*R*)- and (1*S*)-Camphor-Bound P-450$_{cam}$[a]

cation	cation radius (nm)[b]	high-spin content at saturating cation concentration (%)		$K_{d,cat}$ (mM)		saturating cation concentration (mM)	
		(1*R*)-camphor	(1*S*)-camphor	(1*R*)-camphor	(1*S*)-camphor	(1*R*)-camphor	(1*S*)-camphor
Li^+	0.060	84	85	37 ± 3	279 ± 16	326	17000
Na^+	0.095	89	88	24 ± 2	122 ± 7	275	3450
K^+	0.133	100	100	12 ± 1	20 ± 1	122	245
Rb^+	0.148	96	100	15 ± 1	30 ± 3	201	885
Cs^+	0.169	94	95	20 ± 2	59 ± 4	315	2120

[a] Values for (1*R*)-camphor are refitted with the Hill equation from Deprez et al. (1994a). [b] From D'Ans and Lax (1967).

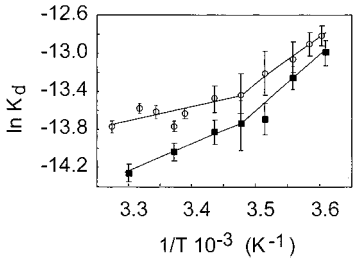

FIGURE 4: Plot of the logarithm of the apparent substrate dissociation constant K_d versus the reciprocal temperature in P-450$_{cam}$. (■) substrate (1*R*)-camphor and (○) substrate (1*S*)-camphor, in 0.1 M potassium phosphate, pH 7.0, 0% (by mass) glycerol. Error bars indicate results of several data sets.

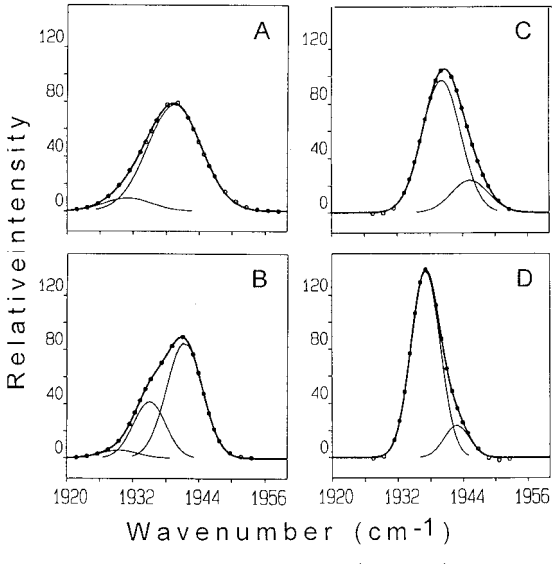

FIGURE 5: CO stretch vibration modes in dependence on the temperature. (1*R*)-camphor-bound P-450$_{cam}$ at (A) 290 K and (B) 20 K. (1*S*)-Camphor-bound P-450$_{cam}$ at (C) 290 K and at (D) 20 K. Measurements were done in 0.1 M potassium phosphate, pH 7.0, 60% (by mass) glycerol, substrate concentration 25 mM, protein concentration 1 mM. The overlapping bands are obtained from curve fitting. The total area is normalized.

metric and can therefore be described by the log-normal distribution line shape as demonstrated by Schulze et al. (1994b). The (1*R*)-camphor-bound complex at room temperature shows one band at 1939.8 cm^{-1} with a width of 12.7 cm^{-1} and an asymmetry parameter $\alpha = 0.93$ indicating the asymmetry at the lower-energy side of the band (Schulze et al., 1994b). In contrast, (1*S*)-camphor-bound P-450$_{cam}$ has the absorption band at 1940.7 cm^{-1}, the width of 9.5 cm^{-1}, and the asymmetry parameter $\alpha = 1.1$, indicating the asymmetry at the higher-energy side of the band. This asymmetry is more strongly pronounced at low temperatures for (1*S*)-camphor, while for (1*R*)-camphor a shoulder at the lower-energy side is revealed.

This behavior indicates the overlap of several substates, which we decomposed with a minimal number of bands for the spectra in the temperature range 20−290 K. For the (1*R*)-camphor-bound protein, two major bands and one minor band are found (Schulze et al., 1994b), while two bands are sufficient to fit the spectrum of the (1*S*)-camphor-bound P-450$_{cam}$. Table 4 summarizes the fit data in 20% and 60% (by mass) glycerol. Three results are important to mention: (i) The bands for the (1*S*)-camphor complex have higher frequencies than those for the (1*R*)-camphor-bound protein. Band 1 at around 1940 cm^{-1} (290 K) is not so strongly shifted to lower values during cooling to 20 K [1937.2 cm^{-1} in the (1*S*)-camphor-bound protein as compared to 1934.8 cm^{-1} for (1*R*)-camphor P-450$_{cam}$ in 60% (by mass) glycerol]. (ii) No strong population exchange between the substates is observed for (1*S*)-camphor compared to its optical antipode (Figure 6 ; Table 4). (iii) The bandwidth is smaller in (1*S*)-camphor P-450 (Table 4).

Assigning that the band at 260 K at 1939.8 cm^{-1} in (1*S*)-camphor P-450$_{cam}$ corresponds to the band at 1938.4 cm^{-1} in the (1*R*)-camphor protein (band 1), the enthalpy and entropy differences for the substate transition from the band 2 to the band 1 show significant differences between both enantiomer complexes (Table 5). While the transition from the band 2 to the band 1 in 60% (by mass) glycerol is enthalpy-driven in the (1*S*)-camphor-bound protein, the entropy term is more dominating in (1*R*)-camphor-P-450$_{cam}$. Population exchange between the substates is observed only above the glass transition temperature (180 K) (Schulze et al., 1994b).

pH Dependence of CO Stretch Vibration. The CO stretch band parameters depend on the solvent condition. The decrease of the pH value shifts the CO stretch vibration to lower frequency along an S-shaped curve with p*K* of 6.2 for (1*R*)-camphor (Schulze et al., 1994b) and p*K* of 6.5 for (1*S*)-camphor.

Influence of Cation Binding on CO Stretch Vibration. Although a specific cation effect on the frequency of the CO stretch vibration with a preferential binding of potassium cations is observed for (1*R*)-camphor (Schulze et al., 1994b), no such dependence was found for (1*S*)-camphor (Figure 7). The frequency of the CO stretch band (log-normal fit) at room temperature averaged over all cations with concentrations between 5 and 350 mM is 1940.7 ± 0.2 cm^{-1}.

DISCUSSION

Several studies have shown that the CO stretch mode is a sensitive spectroscopic probe for the active site in cytochrome P-450 (Jung et al., 1996; Schulze et al., 1994b; Tsubaki et al., 1992; Jung et al., 1992; Jung & Marlow, 1987; Böhm et al., 1979; O'Keefe et al., 1978). While for myoglobins and

Table 4: Fit Data of the Frequencies of the CO Stretch Vibration in (1*R*)- and (1*S*)-Camphor-Bound P-450$_{cam}$

	20 K			260 K		290 K	
20% (by mass) glycerol −buffer							
(1*S*)-camphor		1	2	1	2	1	2
ν_{CO} (cm^{-1})		1937.2	1942.5	1939.7	1944.4	1940.2	1946.3
$\Delta\nu_{1/2}$ (cm^{-1})		6.8	6.2	7.1	7.1	8.6	6.7
population (%)		92	8	89	11	89	11
(1*R*)-camphor	0	1	2	0	1	2	1	0
ν_{CO} (cm^{-1})	1930	1933.8	1941.9	1930	1939.3	1942.5	1939.7	1930.0
$\Delta\nu_{1/2}$ (cm^{-1})	8.6	9.8	7.0	8.6	11.3	6.9	11.9	8.6
population (%)	8	45	47	6.5	91	2.5	95	5
60% (by mass) glycerol−buffer							
(1*S*)-camphor		1	2	1	2	1	2
ν_{CO} (cm^{-1})		1937.2	1942.8	1939.8	1945.8	1940.2	1945.4
$\Delta\nu_{1/2}$ (cm^{-1})		6.3	5.6	7.8	6.7	8.3	8.0
population (%)		87	13	92	8	80	20
(1*R*)-camphor	0	1	2	0	1	2	1	0
ν_{CO} (cm^{-1})	1930	1934.8	1942.7	1930	1938.4	1942.9	1939.3	1930.0
$\Delta\nu_{1/2}$ (cm^{-1})	5.2	7.4	7.1	6.5	10	9.1	11.1	6.5
population (%)	4−0	15−29	85−66	3	77	20	96	4

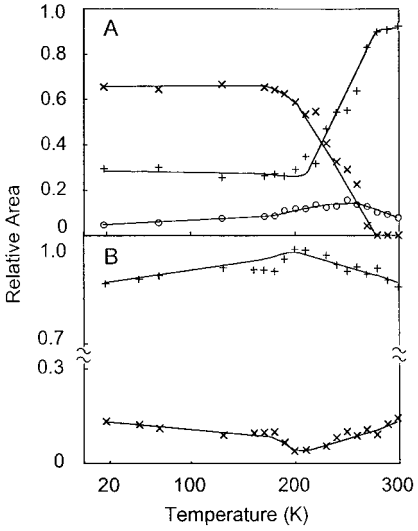

FIGURE 6: Population change of the CO stretch vibration absorption bands with temperature. (A) (1*R*)-Camphor-bound P-450$_{cam}$ and (B) (1*S*)-camphor-bound P-450$_{cam}$ in 0.1 M potassium phosphate, pH 7.0, 60% (by mass) glycerol, substrate concentration 25 mM, protein concentration 1 mM: (○) band 0, (+) band 1, and (×) band 2 (Table 4).

hemoglobins, many studies have revealed that the orientation (Ormos et al., 1988; Li & Spiro, 1988) and the polarizing effect of the distal histidine on the CO ligand is responsible for the CO stretch frequency and the appearance of the three subconformers (Ivanov et al., 1994; Springer et al., 1994; Ray et al., 1994; Li et al., 1994; Sakan et al., 1993; Oldfield et al., 1991), the structural assignment of the CO stretch modes in cytochrome P-450 is not clear to date.

In particular, a significant effect of the binding of various substrates on the frequency of the CO stretch vibration and substate population has been found (Jung et al., 1992), and it has been suggested that this effect might reflect binding properties like substrate mobility and water rearrangements in the heme pocket. A phenomenological classification of the CO stretch infrared spectra has been proposed depending on the kind of binding of the substrates in the heme pocket (Jung et al., 1992). Substrates, which are bound to Tyr96 via a hydrogen bond show one band of varying frequency at room temperature while substrates, which lack this hydrogen bond show a broader spectrum of overlapping bands due to substrate disorder. However, Schulze et al. (1994b) demonstrated for (1*R*)-camphor that even the hydrogen-bonded substrates induce CO ligand subconformers when solvent conditions, temperature, and pressure are changed in a broad range. For a deeper understanding of the kind of information one can obtain from the CO stretch infrared spectrum about the nature of substrate binding and the active site protein structure we carried out a comparative study of the enantiomers (1*R*)- and (1*S*)-camphor with regard to the CO stretch infrared spectra, spin-state equilibrium, substrate dissociation constants and thermal unfolding. Differences in the physico-chemical parameters observed between both enantiomer P-450$_{cam}$ complexes can be directly related to geometrical differences in the binding mode because optical antipodes have the same physico-chemical properties like dipole moments, polarizability and solubility in non-chiral solvents.

The presented data show that the high-spin state in the (1*S*)-camphor complex is less favored compared to (1*R*)-camphor-bound P-450$_{cam}$. At high glycerol content the differences in the high-spin content are very small and can be only estimated from the temperature dependence study of the spin equilibrium (Table 1). However, the relaxation of the spin equilibrium after a negative temperature jump (fast cooling) still reveals significantly different behavior. In the presence of (1*S*)-camphor, the transition rate from the high-spin state to the low-spin state is significantly higher than in the presence of (1*R*)-camphor. Considering that the low-spin state is induced by ligation of water to the heme-iron as the sixth ligand (Poulos et al., 1986; Thomann et al., 1995), a faster water-rebinding rate is therefore observed for the (1*S*)-camphor complex.

Earlier, Fisher and Sligar (1987) carried out spin-state relaxation studies on P-450$_{cam}$ bound to various substrate analogues by applying a small positive temperature jump from 10 to 13 °C. For the equilibrium P-450$^{os}_{LS}$ $\underset{k_{-1}}{\overset{k_1}{\Longleftrightarrow}}$ P-450$^{os}_{HS}$ they found a correlation between the microscopic rate constant k_{-1} and the percentage of initial low-spin character induced by the substrate analogues at the reference temperature of 20 °C. The microscopic rate constant k_{-1} describes the transition from the high-spin state to the low-spin state, and therefore k_{-1} represents the water on-rate. A

Table 5: Thermodynamic Parameters for Conformational Substates of the (1*S*)- and (1*R*)-Camphor-Bound P-450$_{cam}$−CO Complex[a,b]

	ΔE_i (kJ/mol)	ΔS_i (J/molK)	Δs_i	ΔH^c (kJ/mol)	ΔS^c (J/mol K)
		results for 20% (by mass) glycerol−buffer for 200−260 K			
(1*S*)-camphor					
1	−2.1 ± 1.6	9 ± 6	−0.22 ± 0.2	−5.1	−1.7
2	0	0	0	0	0
(1*R*)-camphor					
0	25.7 ± 5.0	107.5 ± 21	−0.30 ± 1	21.7	93.1
1	26.2 ± 4.4	130.2 ± 18	1.85 ± 1	50.5	219.0
2	0	0	0	0	0
		results for 60% (by mass) glycerol−buffer for 220−280 K			
(1*S*)-camphor					
1	−10.9 ± 0.7	−23.8 ± 2.6	−0.66 ± 0.1	−19.6	−55.5
2	0	0	0	0	0
(1*R*)-camphor					
0	24.5 ± 7.4	81.9 ± 29.4	−1.04 ± 3.0	10.8	31.6
1	22.0 ± 1.2	96.7 ± 4.9	3.1 ± 0.4	63.4	247.5
2	0	0	0	0	0

[a] Fit results for ΔE_i and ΔS_i (250 K,0.1 MPa) from $\Delta S_i(T,p) = \Delta S_i(250,0.1) + \Delta s_i T + \Delta v_i p$; $\Delta V_i(T,p) = \Delta V_i(250,0.1) - \Delta v_i T + \Delta q_i p$; $\Delta H_i(T,p) = \Delta E_i(250,0.1) + p\Delta V_i(250,0.1) + {}^1/_2\Delta s_i T^2 + {}^1/_2\,\Delta q_i p^2$ with ΔE_i, ΔH_i, ΔS_i, ΔV_i, Δs_i referring to the difference for substates (i) for internal energy, enthalpy, entropy, volume, and for entropy change, respectively. Δv_i and Δq_i are related to isobar thermal expansion coefficient and isothermal compressibility, respectively, and were set to zero for constant pressure 0.1 MPa (Jung & Marlow, 1987; Jung et al., 1996). [b] Zero values indicate the reference substate. [c] Calculated values for ΔH and ΔS at 298 K, 0.1 MPa.

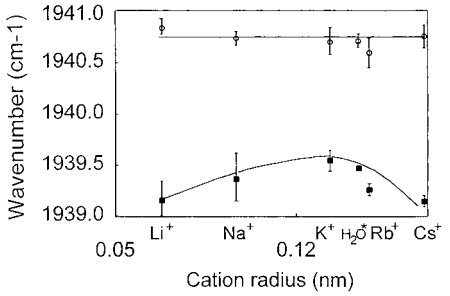

FIGURE 7: Mean values of the frequency of the CO stretch vibration in dependence on the radius of the non-hydrated cations Li^+, Na^+, K^+, Rb^+, Cs^+ (D'Ans & Lax, 1967) and a water molecule H_2O^* (Kundrot & Richards, 1988). Error bars are obtained from measurements at varying cation concentrations (5−350 mM). (■) (1*R*)-Camphor and (○) (1*S*)-camphor, in 50 mM Tris-HCl, pH 7.5, 20% (by mass) glycerol, saturating substrate concentration 400 μM at 28.5 °C.

higher initial low-spin state population or a higher water content in the active site respectively correlates with a larger value for the water on-rate. Although this conclusion was drawn from studies in the small temperature range (10−13 °C) it can be applied to a wider temperature range. Our negative temperature jump study clearly reveals that there is a higher water on-rate for the (1*S*)-camphor complex, and therefore a higher water content may be concluded.

Increasing hydrostatic pressure leads to a contraction of the protein structure by pushing water into the protein interior (Kharakoz & Sarvazyan, 1993). For P-450$_{cam}$ it was found that the spin reaction volume change is a thermodynamic parameter, which reflects a measure of the initial (0.1 MPa) water content in the heme-iron environment (Hui Bon Hoa & Marden, 1992b; Deprez et al., 1994b). A smaller spin reaction volume difference measured using the high-pressure technique correlates for several substrate analogue P-450$_{cam}$ complexes with a larger initial low-spin content (0.1 MPa) and therefore with a higher initial water content. We would like to attribute the measured spin reaction volume difference to changes in the number of water molecules interacting with the substrate in the heme pocket. However, we do not know which value to use for the partial molar volume of water in the hydrophobic active site. Using the partial molar volume of water at 0.1 MPa (ΔV_{H_2O} = 18 cm^3/mol) will probably underestimate the number of water molecules interacting in the active site (Jung et al., 1995; Di Primo et al., 1992). It allows us to evaluate roughly the magnitude of the water content between both enantiomeric substrate-bound cytochrome P-450$_{cam}$ complexes. The spin reaction volume difference found for (1*S*)-camphor-bound P-450$_{cam}$ is 16 ± 9 cm^3/mol smaller as compared to the (1*R*)-camphor-bound complex (Table 2). This result suggests that the (1*S*)-camphor-bound P-450$_{cam}$ has a slightly higher water content in the heme pocket or generally in the protein than the (1*R*)-camphor-bound complex. The lower half-transition pressure of (1*S*)-camphor might support this finding.

Thus, both methods, namely the high-pressure and the kinetic studies, lead to the conclusion that the (1*S*)-camphor-bound P-450$_{cam}$ has a higher water content.

On substrate binding water is exposed from the heme-iron of the substrate-free P-450$_{cam}$. A lower substrate association constant (or a higher substrate dissociation constant) which is found for (1*S*)-camphor can be interpreted by a less optimal binding in the active site. We suppose less tight substrate−protein active site contacts. As recently discussed by Kadkhodayan et al., (1995), (1*S*)-camphor may still be oriented by the hydrogen bond between its carbonyl group and the Tyr96OH. Because (1*S*)-camphor reacts exclusively at the exo-position of C-5 (Kadkhodayan et al., 1995; Maryniak et al., 1993), the hydrogen atoms of C-3 may occupy the position where the 10-methyl group is located in (1*R*)-camphor, leading to modified substrate−protein interactions, especially to the I-helix (Raag & Poulos, 1989; Poulos et al., 1987). Hence, on substrate dissociation less contacts have to be broken to expose the substrate and to facilitate the entry of water to the heme-iron environment. The water-rebinding process (thermodynamic and kinetic parameters) is obviously described by the substrate dissociation process. Thus, a higher substrate dissociation constant is related to a higher water on-rate.

The mentioned water on-rate is also reasonable to use as a direct measure for the increased water mobility, which is

caused by the protein flexibility. Because bound substrates have distinct contacts to the protein, the flexibility of the protein might reflect also the freedom of substrate movements. Hence, the water on-rate, but also the substrate dissociation constant, might be in relationship with the substrate mobility.

A less optimal binding and the supposed higher mobility of the substrate would also explain the larger dissociation constants for the cations, $K_{d,cat}$ (Table 3), for the (1*S*)-camphor-bound P-450$_{cam}$. In the crystal structure of oxidized (1*R*)-camphor-bound P-450$_{cam}$, Poulos et al. (1987) found an octahedral arrangement of the oxygen atoms of four carbonyl groups of the amino acids Glu84, Gly93, Glu94, and Tyr96 and two water molecules (517 and 584) which form a cage for a molecule assigned as "solvent" molecule 515. Studies by Deprez et al.(1994a), Di Primo et al. (1992), Lange et al. (1979), and Peterson (1971) led to the suggestion that the cage is occupied by a cation. Potassium cations are preferentially bound (Deprez et al., 1994a) and stabilize the (1*R*)-camphor binding geometry. Conversely, camphor binding also stabilizes the cation binding (Deprez et al., 1994a). A more loosely bound substrate or a substrate bound in a different geometry should therefore stabilize the cation binding to a lower extent, as we see for (1*S*)-camphor-bound P-450$_{cam}$.

The half-transition temperature for thermal unfolding is 1 degree lower in the presence of (1*S*)-camphor ($T_{1/2}$ = 53.8 °C) compared to (1*R*)-camphor ($T_{1/2}$ = 54.8 °C). Jung et al. (1985, 1994) have shown three unfolding units for P-450$_{cam}$ with transition temperatures at 41.9, 47.8, and 54.3 °C in the absence of substrates and at 48.5, 57.8, and 61.7 °C in the presence of (1*R*)-camphor. Three structural domains have been proposed from analyzing the P-450$_{cam}$ crystal structure for the localization of hydrophobic cores and possible hydrophilic domain interfaces (Jung et al., 1994). The heme is located in the contact region of all three domains. The binding of (1*R*)-camphor stabilizes the protein structure due to its contact to domains I and III. One can imagine that this contact is loosened in the (1*S*)-camphor-bound protein due to a changed binding geometry of this enantiomer.

Because a crystal structure of the (1*S*)-camphor complex is still not available, which would support or exclude our conclusions, we modeled (1*S*)-camphor into the active site so that it made a hydrogen bond to Tyr96. Molecular dynamics simulations were performed under the same conditions as in previous work (Helms et al., 1996) at 300 K for both (1*S*)- and (1*R*)-camphor. Simulations were done for 100 ps allowing a 15 Å radius sphere of atoms (930 atoms) around the geometric center of the active site to be free, harmonically restraining an additional 2 Å shell of atoms, and fixing the remaining 3070 atoms. The protein was solvated by a 28 Å shell of water molecules. The root mean square fluctuation of the substrate (1*S*)-camphor is larger (0.9 Å) compared to (1*R*)-camphor (0.55 Å). These simulations indicate that (1*S*)-camphor is more mobile than (1*R*)-camphor. However, in contrast to our expectation from the experimental data, the active site amino acid residues retain similar conformations and dynamics in these simulations. Thus, the simulations indicate that longer-range dynamic effects than could be accounted for in molecular dynamics simulations of the active site region have to be considered to explain the larger water accessibility and protein flexibility of the (1*S*)-camphor complex compared to (1*R*)-camphor-bound cytochrome P-450$_{cam}$.

Under consideration of these results of the simulations we should also consider that the estimated difference of the transition volume for the high-spin/low-spin equilibrium between both enantiomer complexes may result from a net effect of a higher number of water molecules in the protein structure of the (1*S*)-camphor complex and not necessarily from additional distinct water molecules in the heme pocket. Recent studies of the hydrostatic pressure-induced red shift of the Soret band in P-450$_{cam}$−CO bound with various substrates and its correlation to the low-spin state content indicate that one should also consider a more global electrostatic effect, which would include water and polar amino acids in the protein nearer to and further away from the direct heme pocket (Jung et al., 1995). From our studies we cannot differentiate between these different possibilities. Summarizing the conclusions drawn from the studies on the oxidized form of P-450$_{cam}$, we suggest that (1*S*)-camphor is more loosely bound in the heme pocket and the access of water molecules from the bulk solvent to the heme environment is facilitated.

One may ask whether the higher mobility and the higher water content for the (1*S*)-camphor-bound P-450$_{cam}$ would be reflected also in the ferrous CO-bound protein?

The infrared spectrum of the (1*S*)-camphor P-450$_{cam}$-CO complex reveals distinct differences to the spectrum of the (1*R*)-camphor complex: (i) the CO stretch bands have slightly but significantly higher frequencies (by about 1−2 cm^{-1}) and do not show such a strong temperature dependent frequency shift, and there is no cation effect on the frequency; (ii) there is no strong population exchange between the substates; and (iii) the bandwidth is smaller (by 2−4 cm^{-1}).

To clarify point i we consider the arguments of recent extensive infrared, resonance Raman, and X-ray crystallography studies and molecular dynamics simulation on wild type and mutated myoglobin (Li et al., 1994; Jewsbury & Kitagawa, 1994, 1995; Sakan et al., 1993). They have demonstrated that the polarising effect of the distal heme surrounding the CO ligand dipole is the determining physical parameter for the CO stretch frequency. Positive electrostatic fields near the CO ligand should favor the resonance form $Fe^{\delta(+)}{=}C{=}O^{\delta(-)}$, corresponding to a decreased frequency, while negative electrostatic fields should induce the inverse effect with the resonance form $Fe^{\delta(-)}{-}{-}{-}C{\equiv}O^{\delta(+)}$ and higher frequencies (Kushkuley & Stavrov, 1996; Li at al., 1994; Li & Spiro, 1988). A positive electrostatic field induced by a proton attachment or hydrogen bonding from Thr252OH to the CO ligand has already been excluded for the (1*R*)-camphor-bound P-450$_{cam}$ (Kimata et al., 1995; Schulze et al., 1994b) and may also not be the case for the (1*S*)-camphor complex. The observed pH effect on the CO stretch mode for both enantiomer complexes seems to be a secondary effect on the protein structure because the same p*K* values are observed for the CO complex as well as for the oxidized protein. However, an effective positive electrostatic field near the oxygen atom of the CO ligand, which stabilizes the CO binding but does not result from a hydrogen bond, has to be assumed in the (1*R*)-camphor complex (Kushkuley & Stavrov, 1996). Instead of a hydrogen bond an electrostatic interaction (contact) of the CO with a polar patch around Thr252 in the I-helix on the distal side is supposed. In the (1*S*)-camphor complex the positive electrostatic potential is

partially compensated by the electric field of an increased water content, which results in a weakening of this contact as recently discussed by Jung et al. (1996). The weaker contact from CO to the I-helix is reflected in the slightly higher CO stretch frequency.

A possible generally decrease of the electron-donating capacity of the negatively charged cysteine iron ligand on the proximal side, which would also result in a higher CO frequency (Jung, 1983), is excluded because various substrate analogues, including (1*S*)-camphor complexes, fall on the same line in the plot of the ^{12}CO stretch frequency against the ^{13}CO NMR chemical shift (Legrand et al., 1995).

The supposed weaker contact of the CO ligand to the I-helix in the (1*S*)-camphor complex would also explain the negligible frequency shift with decreasing temperature and the missing cation effect, which, in the case of (1*R*)-camphor complex, is transmitted to the CO ligand in a concerted action of the substrate and the protein via van der Waals contact between the 10-methyl group of (1*R*)-camphor and Val247 in the I-helix (Raag & Poulos, 1989; Poulos et al., 1987). This van der Waals contact seem to be not optimal in the (1*S*)-camphor complex.

The negligible substate interconversion (ii) in the (1*S*)-camphor complex supports that the CO ligand has a weaker contact to the I-helix, otherwise the CO substates would follow the temperature-induced conformational changes of the protein (Doster et al., 1986).

The smaller width of the CO stretch mode infrared band in (1*S*)-camphor-bound P-450$_{cam}$ (iii) would suggest that the active site is more rigid. This is only in the first view contradictionary to our conclusions of a higher mobility of (1*S*)-camphor compared to (1*R*)-camphor. For diverse metal carbonyl complexes Beck and Lottes (1964) have shown that an increase of the polarity of the solvent induces a lowering of the CO stretch frequency and a broadening of the vibration band due to increased contacts of the solvent molecules with the CO ligand. This contact causes the annihilation of the accidental energetic degeneracy of the intermolecular vibrational states reflected in an increase of the width (inhomogeneous broadening) (Dodson et al., 1996). This phenomenon is usually used as an indication of a higher mobility of the solvent−CO contact region where the complex fluctuates between many microstates. In our case, however, we conclude that the mobility of (1*S*)-camphor results in a higher accessibility of the protein structure for water molecules, which have no direct contact to the CO ligand but which have an indirect influence on the CO via the partial compensation of the positive electrostatic potential, resulting in a weakening the contact of CO to the I-helix. So the width of the CO stretch band may not be a relevant parameter to describe the mobility of the substrate. This explanation, however, needs further verification.

Molecular dynamic simulations were also performed for the CO-bound P-450$_{cam}$ complex in the presence of (1*R*)- and (1*S*)-camphor. The analysis of the simulations shows that (1*S*)-camphor has no sterically different effect on the CO from (1*R*)-camphor, indicating that the CO stretch frequency shift should be due to a change in polarity rather than due to sterical constraints. The mobility and positions of the amino acid residues around the active site, the volume of the active site, and the regions favorable for hydration as detected by GRID analysis (GRID v. 12, Molecular Discovery Ltd., West Way House, Elms Parade, Oxford OX2 0LL, England) are similar. This indicates that there are no pronounced differences in the side chain conformers or the degree of hydration of the active site. However, the rms fluctuation for the substrate is larger for (1*S*)-camphor (0.97 Å) as compared to (1*R*)-camphor (0.58 Å), as it is seen for the oxidized protein.

Thus the mobility of (1*S*)-camphor is maintained after reduction and CO binding. This conclusion is supported by our recent comparative study of the rebinding kinetics of the photodissociated CO ligand in P-450$_{cam}$ bound with (1*S*)- and (1*R*)-camphor using time-resolved infrared spectroscopy (Contzen et al., 1996).

Summarizing all of the results and conclusions presented in this paper, we suggest that (1*S*)-camphor is bound in the heme pocket of oxidized P-450$_{cam}$ with a modified geometry, with a higher mobility, and with a stronger accessibility of the protein structure for solvent molecules. In the reduced protein the higher water content decreases the influence of the positive electrostatic field acting on the CO ligand, which results in a weaker polar contact of the CO ligand to the protein environment (Jung et al., 1996). Assuming that the CO complex represents a model for the dioxygen complex, we speculate that the higher amount of uncoupling observed for (1*S*)-camphor conversion by P-450$_{cam}$ [11% compared to 3% for (1*R*)-camphor; Kadkhodayan et al., 1995; Maryniak et al., 1993] may be a consequence of the weaker stabilization of the dioxygen ligand due to loosening polar contacts to the I-helix. This conclusion is in agreement with site-directed mutagenesis studies (Kimata et al., 1995; Shimada et al., 1991; Imai et al., 1989; Martinis et al., 1989; Raag & Poulos, 1991) showing increased uncoupling by substituting the polar Thr252 to apolar amino acids.

ACKNOWLEDGMENT

We gratefully thank Dr. Otto Ristau for his assistance in fitting the experimental data. We are very grateful to Dr. K.-L. Schröder for running the fermentor for the *Escherichia coli* culture and to Gisela Sklenar for purifying cytochrome P-450$_{cam}$.

REFERENCES

Atkins, W. M., & Sligar, S. G. (1988) *J. Biol. Chem. 263*, 18842−18849.

Atkins, W. M., & Sligar, S. G. (1989) *J. Am. Chem. Soc. 111*, 2715−2717.

Beck, W., & Lottes, K.-M. (1964) *Z. Naturforsch. 19b*, 987−994.

Böhm, S., Rein, H., Butschak, G., Scheunig, G., Billwitz, H., & Ruckpaul, K. (1979) *Acta Biol. Med. Ger. 38*, 249−255.

Contzen, J., Ristau, O., & Jung, C. (1996) *FEBS Lett. 383*, 13−17.

Cupp-Vickery, J. R., Li, H., & Poulos, T. L. (1994) *Protein 20*, 197−201.

D'Ans, J., & Lax, E. (1967) *Taschenbuch für Chemiker und Physiker*, 3rd ed., Springer Verlag, Berlin.

Davydov, D. R., Deprez, E., Hui Bon Hoa, G., Knyushko, T. V., Kuznetsova, G. P., Koen, Y. M., & Archakov, A. I. (1995) *Arch. Biochem. Biophys. 320*, 330−344.

De Voss, J. J., & Ortiz de Montellano, P. R. (1995) *J. Am. Chem. Soc. 117*, 4185−4186.

Deprez, E., Di Primo, C., Hui Bon Hoa, G., & Douzou, P. (1994a) *FEBS Lett. 347*, 207−210.

Deprez, E., Gerber, N. C., Di Primo, C., Douzou, P., Sligar, S. G., & Hui Bon Hoa, G. (1994b) *Biochemistry 33*, 14464−14468.

Di Primo, C., Hui Bon Hoa, G., Douzou, P., & Sligar, S. G. (1992) *Eur. J. Biochem. 209*, 583−588.

Dodson, E. D., Zhao, X.-J., Caughey, W. S., & Elliott, C. M. (1996) *Biochemistry 35*, 444−452.

Doster, W., Bachleitner, A., Dunau, R., Hiebl, M., & Lüscher, E. (1986) *Biophys. J. 50*, 213−219.
Douzou, P. (1977) *Cryobiochemistry: An Introduction*, Academic Press, London.
Fisher, M. T., & Sligar, S. G. (1987) *Biochemistry 26*, 4797−4803.
Fowler, S. M., England, P. A., Westlake, A. C. G., Rouch, D. R., Nickerson, D. P., Blunt, C., Braybrook, D., West, S., Wong, L. L., & Flitsch, S. L. (1994) *J. Chem. Soc. Chem. Commun. 24*, 2761−2762.
Frauenfelder, H., Alberding, N. A., Ansari, A., Braunstein, D., Cowen, B. R., Hong, M. K., Iben, I. E. T., Johnson, J. B., Luck, S., Marden, M. C., Mourant, J. R., Ormos, P., Reinisch, L., Scholl, R., Schulte, A., Shyamsunder, E., Sorensen, L. B., Steinbach, P. J., Xie, A.-H., Young, R. D., & Yue, K. T. (1990) *J. Phys. Chem. 94*, 1024−1037.
Fruetel, J., Chang, Y.-T., Collins, J., Loew, G., & Ortiz de Montellano, P. R. (1994) *J. Am. Chem. Soc. 116*, 11643−11648.
Griffin B. W., & Peterson, J. A. (1972) *Biochemistry 11*, 4740−4746.
Gunsalus, I. C., & Sligar, S. G. (1978) in *Advances in Enzymology and Related Areas of Molecular Biology* (Nord, F. F., Ed.) Vol. 47, pp 1−44, Wiley, New York.
Harris, D. L., & Loew, G. H. (1994) *J. Am. Chem. Soc. 116*, 11671−11674.
Hasemann, C. A., Kurumbali, R. G., Boddupali, S. S., Peterson, J. A., & Deisenhofer, J. (1995) *Structure 3*, 41−62.
Helms, V., Deprez, E., Gill, E., Barret, C., Hui Bon Hoa, G., & Wade, R. C. (1996) *Biochemistry 35*, 1485−1499.
Hui Bon Hoa, G., Douzou, P., Dahan, N., & Balny, C. (1982a) *Anal. Biochem. 120*, 125−145.
Hui Bon Hoa, G., & Marden, M. C. (1982b) *Eur. J. Biochem. 124*, 311−315.
Imai, M., Shimada, H., Watanabe, Y., Matsushima-Hibiya, Y., Makino, R., Koga, H., Horiuchi, T.,& Ishimura, Y. (1989) *Proc. Natl. Acad. Sci. U.S.A. 86*, 7823−7827.
Ivanov, D., Sage, T., Keim, M., Powell, J. R., Asher, S. A., & Champion, P. M. (1994) *J. Am. Chem. Soc. 116*, 4139−4140.
Jewsbury, P., & Kitagawa, T. (1994) *Biophys. J. 67*, 2236−2250.
Jewsbury, P., & Kitagawa, T. (1995) *Biophys. J. 68*, 1283−1294.
Jung, C. (1983) *Stud. Biophys. 93*, 225−230.
Jung, C., Bendzko, P., Ristau, O., & Gunsalus, I. C. (1985) in *Cytochrome P-450* (Vereczky, C., & Magyar, K., Eds.), pp 19−22, Akademiai Kiado, Budapest.
Jung, C., & Marlow, F. (1987) *Stud. Biophys. 120*, 241−251.
Jung, C., Ristau, O., & Rein, H. (1991) *Biochim. Biophys. Acta 1076*, 130−136.
Jung, C., Hui Bon Hoa, G., Schröder, K.-L., Simon, M., & Doucet, J. P. (1992) *Biochemistry 31*, 12855−12862.
Jung, C., Pfeil, W., Köpke, K., Schulze, H., & Ristau, O. (1994) in *Cytochrome P-450 8th International Conference* (Lechner, M. C., Ed.) pp 543−546, John Libbey Eurotext, Paris.
Jung, C., Hui Bon Hoa, G., Davydov, D., Gill, E., & Heremans, K. (1995) *Eur. J. Biochem. 233*, 600−606.
Jung, C., Ristau, O., Schulze, H., & Sligar, S. G. (1996) *Eur. J. Biochem. 235*, 660−669.
Kadkhodayan, S., Coulter, E. D., Maryniak, D. M., Bryson, T. A., & Dawson, J. H. (1995) *J. Biol. Chem. 270*, 28042−28048.
Kharakoz, D. P., & Sarvazyan, A. P. (1993) *Biopolymers 33*, 11−26.
Kimata, Y., Shimada, H., Hirose, T., & Ishimura, Y. (1995) *Biochem. Biophys. Res. Commun. 208*, 96−102.
Kundrot, C. E., & Richards, F. M. (1988) *J. Mol. Biol. 200*, 401−410.
Kushkuley, B., & Stavrov, S. S. (1996) *Biophys. J. 70*, 1214−1229.
Lange, R., Hui Bon Hoa, G., Debey, P., & Gunsalus, I. C., (1979) *Eur. J. Biochem. 94*, 491−496.
Legrand, N., Bondon, A., Simonneaux, G., Jung, C., & Gill, E. (1995) *FEBS Lett. 364*, 152−156.
Li, T. L., Quillin, M. L., Phillips, G. N., Jr., & Olson, J. S. (1994) *Biochemistry 33*, 1433−1446.
Li, X. Y., & Spiro, T. G. (1988) *J. Am. Chem. Soc. 110*, 6024−6033.
Loida, P. J., & Sligar, S. G. (1993a) *Biochemistry 32*, 11530−11538.
Loida, P. J., & Sligar, S. G. (1993b) *Protein Eng. 6*, 207−212.
Martinis, S. A., Atkins, W. A., Stayton, P. S., & Sligar, S. G. (1989) *J. Am. Chem. Soc. 111*, 9252−9253.
Maryniak, D. M., Kadkhodayan, S., Crull, G. B., Bryson, T. A., & Dawson, J. H. (1993) *Tetrahedron 49*, 9373.
Nelson, D. R., Kamataki, T., Waxman, D. J., Guengerich, F. P., Estabrook, R. W., Feyereisen, R., Gonzalez, F. J., Coon, M. J., Gunsalus, I. C., & Gotoh, O. (1993) *DNA Cell Biol. 12*, 1−51.
Nölting, B., Jung, C., & Snatzke, G. (1991) *Biochim. Biophys. Acta 1100*, 171−176.
O'Keefe, D. H., Ebel, R. E., Peterson, J. A., Maxwell, J. C., & Caughey, W. S. (1978) *Biochemistry 26*, 5845−5852.
Oldfield, E., Guo, K., Augspurger, J. D., & Dykstra, C. E. (1991) *J. Am. Chem. Soc. 113*, 7537−7541.
Ormos, P., Braunstein, D., Frauenfelder, H., Hong, M. K., Lin, S.-L., Sauke, T. B., & Young, R. D. (1988) *Proc. Natl. Acad. Sci. U.S.A. 85*, 8492−8496.
Paulsen, M. D., Filipovic, D., Sligar, S. G., & Ornstein, R. L. (1993) *Protein Sci. 2*, 357−365.
Peterson, J. A. (1971) *Arch. Biochem. Biophys. 144*, 678−693.
Poulos, T. L., Finzel, B. C., & Howard, A. J. (1986) *Biochemistry 25*, 5314−5322.
Poulos, T. L., Finzel, B. C., & Howard, A. J. (1987) *J. Mol. Biol. 195*, 687−700.
Raag, R., & Poulos, T. L. (1989) *Biochemistry 28*, 7586−7592.
Raag, R., & Poulos, T. L. (1991) *Biochemistry 30*, 11420−11429.
Raag, R., & Poulos, T. L. (1992) in *Relationship between Structure and Function of Cytochrome P-450: Experiments, Calculations, Models* (Ruckpaul, K., & Rein, H., Eds.) Frontiers in Biotransformation 7, pp 23−26, Akademie Verlag, Berlin.
Ray, G. B., Li, X-X., Ibers, J. A., Sessler, J. L., & Spiro, T. G. (1994) *J. Am. Chem. Soc. 116*, 162−176.
Sakan, Y., Ogura, T., Kitagawa, T., Fraunfelter, F. A., Mattera, R., & Ikeda-Saito, M. (1993) *Biochemistry 32*, 5815−5824.
Schulze, H., Ristau, O., & Jung, C. (1994a) *Biochim. Biophys. Acta 1183*, 491−498.
Schulze, H., Ristau, O., & Jung, C., (1994b) *Eur. J. Biochem. 224*, 1047−1055.
Schulze, H., Ristau, O., & Jung, C., (1994c) in *Cytochrome P-450 8th International Conference* (Lechner, M. C., Ed.) pp 595−598, John Libbey Eurotext, Paris.
Shimada, H., Makino, R., Imai, M., Horiuchi, T., & Ishimura, Y. (1991) in *International Symposium on Oxygenase and Oxygen Activation* (Yamamoto, S., Nozaki, M., & Ishimura, Y., Eds.) pp.133−136, Yamada Science Foundation, University of Tokyo Press, Tokyo.
Springer, B. A., Sligar, S. G., Olson, J. S., & Phillips, G. N. (1994) *J. Chem. Rev. 94*, 699−714.
Thomann, H., Bernado, M., Goldfarb, D., Kroneck, P. M. H.,& Ullrich, V. (1995) *J. Am. Chem. Soc. 117*, 8243−8251.
Tsubaki, M., Yoshikawa, S., Ichikawa, Y., & Yu, N.-T. (1992) *Biochemistry 31*, 8991−8999.
Tuck, S. F., Graham-Lorence, S., Peterson, J. A.,& Ortiz de Montellano, P. R. (1993) *J. Biol. Chem. 268*, 269−275.

BI9527303